Journal of Materials Research and Technology 42 (2026) 3367–3375

Contents lists available at ScienceDirect

Journal of Materials Research and Technology

journal homepage: www.elsevier.com/locate/jmrt

Influence of PEO regime on sol-gel infiltration and performance of hybrid organic-inorganic coatings on AZ31 alloy

Lara Moreno [a,*], Alexandre Mégret [b], Yoann Paint [c], Marie-Georges Olivier [a,c]

[a] Materials Science Department, University of Mons, 20 Place du Parc, 7000, Mons, Belgium
[b] Metallurgy Department, University of Mons, 20 Place du Parc, 7000, Mons, Belgium
[c] Materia Nova Research Center, Parc Initialis, 7000, Mons, Belgium

ARTICLE INFO

Keywords:
Magnesium
Plasma electrolytic oxidation
Arc regime
Soft regime
Sol-gel
Duplex coatings

ABSTRACT

Magnesium alloys are considered for industrial applications due to their low density and high specific strength. However, their high corrosion susceptibility remains a limitation, necessitating the development of effective surface protection strategies. In this study, AZ31 alloy was modified using hybrid zirconium-silicon sol-gel coatings (ZTP), plasma electrolytic oxidation (PEO) layers produced under arc (PEO-AR) and soft (PEO-SR) regimes, and combined PEO/ZTP duplex systems. The coatings were characterized in terms of morphology, composition, and mechanical behaviour. FTIR analysis confirmed the formation of an inorganic-organic hybrid network based on Zr–O–Si, Si–O–Si and Zr–O–Zr linkages, whereas rheological measurements revealed constant behaviour with ageing time (~11.8 mPa·s), favouring controlled pore infiltration. SEM/EDS analyses confirmed the formation of porous PEO layers and the deposition of a uniform sol-gel coating on AZ31, while the duplex systems displayed different structural architectures. The PEO-AR/ZTP coating reached 11.41 μm, reflecting extensive sol-gel penetration into the large, open pores of the oxide layer. While, the PEO-SR/ZTP coating exhibited a thicker duplex structure (28.4 μm), but sol-gel infiltration remained largely superficial due to the finer and more compact pore network of the PEO layer. Tribological testing revealed that the PEO-AR/ZTP coating achieved the lowest coefficient of friction (~0.35) and superior wear resistance, whereas the PEO-SR/ZTP coating exhibited partial layer detachment and progressive degradation during sliding. These show that sol-gel infiltration depth and PEO pore architecture are key to the mechanical integrity and durability of duplex coatings, providing a framework for the design of hybrid protective systems for magnesium alloys.

1. Introduction

Magnesium and its alloys have attracted increasing attention as strategic materials for lightweight structural applications, particularly in the transportation, aerospace, and energy sectors. Their exceptionally low density (~1.74 g/cm^3), combined with high specific strength (up to 350 MPa) and stiffness, make them promising alternatives to aluminium and steel for reducing component weight and improving fuel efficiency [1,2]. These properties are especially relevant for automotive and aerospace design, where weight reduction directly contributes to lower energy consumption and reduced CO_2 emissions by up to 15-20% compared to conventional materials [3–5]. Moreover, magnesium alloys possess superior damping capacity (5-10 times higher than aluminium), excellent machinability, and good electromagnetic shielding properties, further extending their potential in advanced engineering applications [6]. However, despite these advantages, their high chemical reactivity and poor corrosion resistance in humid or saline environments with corrosion rates reaching 10-50 mm/year in marine conditions remain major obstacles to widespread adoption [7–9].

Surface protection is therefore critical to stabilizing magnesium alloys under service conditions. Among the various surface modification techniques proposed, including anodising, conversion coatings, physical vapour deposition, and thermal oxidation; plasma electrolytic oxidation (PEO) has emerged as one of the most effective and environmentally sustainable methods for improving corrosion and wear resistance [10]. PEO, also known as micro-arc oxidation (MAO), is an electrochemical process conducted at high voltages (typically 150-800 V) and current densities (1-50 A/dm^2), during which intense plasma discharges occur at the metal/electrolyte interface [11]. These discharges locally heat the surface to temperatures exceeding 2000-4000 °C, promoting *in situ*

* Corresponding author.
E-mail address: lara.moreno95@hotmail.com (L. Moreno).

https://doi.org/10.1016/j.jmrt.2026.03.285
Received 5 February 2026; Received in revised form 18 March 2026; Accepted 31 March 2026
Available online 3 April 2026

oxidation and the formation of a hard, adherent ceramic coating with thickness ranging from 5 to 200 μm [12]. The resulting layer typically presents a duplex structure: a dense inner barrier layer (1-10 μm) that provides corrosion resistance and an outer porous region (10-100 μm) that improves mechanical interlocking and allows for secondary functionalization [13]. ·Unlike conventional anodising, PEO uses environmentally alkaline electrolytes and can incorporate species such as Si, Zr, P, or Ca directly from the electrolyte into the growing oxide film, enhancing both corrosion resistance and mechanical properties.

The microstructure and performance of PEO coatings strongly depend on the electrical regime applied during processing. The conventional arc regime involves strong plasma discharges that generate large molten pools and result in relatively thick but rough coatings, with heterogeneous pore distribution, surface roughness (R_a = 2-8 μm), and open porosity (10-30%) that may compromise long-term protection. In contrast, the soft-sparking regime operates under lower current densities (typically <10 A/dm^2) or controlled current waveforms that moderate plasma energy, producing finer discharges and coatings with reduced surface roughness (R_a = 0.5-2 μm) and porosity (5-15%) [14,15]. Recent studies have shown that soft-sparking conditions promote more uniform discharge activity, and improved oxide-layer compactness, resulting in better adhesion and enhanced corrosion-barrier performance [16].

However, despite these advances in understanding PEO formation mechanisms, significant challenges remain. Recent work by Pietrzyk et al., on soft-sparking mechanisms revealed that it represents a dynamic equilibrium state that remains ambiguous in terms of its role in oxide-layer formation, particularly for magnesium substrates where the phenomenon is less well-characterized compared to aluminium alloys [17]. Furthermore, the relationship between processing parameters and coating microstructure remains unclear, especially for complex, multi-step processes. The authors emphasise that the impact of different parameters on the formation and properties of PEO coatings requires more systematic research [18]. Despite the benefits of compact coatings obtained in soft regimes, both arc and soft processes are still affected by the intrinsic presence of interconnected microdefects, which allow electrolyte ingress during operation. This ultimately leads to the degradation of the protective barrier and substrate corrosion, with impedance values typically in the range of 10^3-10^5 Ω·cm^2 [19,20]. Therefore, although PEO coatings offer significantly greater protection than untreated surfaces, they remain susceptible to deterioration when exposed to aggressive environmental conditions over the long term.

In order to solve these limitations, considerable research efforts have been directed towards the development of post-treatment strategies aimed at sealing the intrinsic porosity of PEO coatings [21]. Current approaches involve the infiltration of the porous PEO layer with different functional materials, including polymers, corrosion inhibitors, nanoparticles, and inorganic, organics, or hybrid coatings [22–25]. These treatments are designed to block interconnected pores and microcracks, reduce electrolyte penetration, and improve the overall barrier performance of the coating system. Among the various strategies reported in the literature, hybrid organic-inorganic layers have shown promising results in enhancing corrosion resistance by forming additional barrier layers within the porous PEO structure. Among these approaches, sol-gel-based sealing treatments have attracted particular attention due to their ability to infiltrate fine pore networks and form dense inorganic or hybrid oxide layers that strongly adhere to the PEO substrate.

Sol-gel sealing treatments have been widely investigated as a post-processing strategy to enhance the protective performance of PEO coatings [26,27]. Sol-gel technology involves the hydrolysis and condensation of metal alkoxides or hybrid inorganic-organic precursors to form dense, amorphous oxide networks with tuneable porosity and controllable thickness (1-20 μm) [28–31]. The process can be carried out at low temperatures, ensuring excellent compatibility with pre-existing oxide films and minimal thermal stress. When applied over PEO coatings, sol-gel layers infiltrate and seal surface pores and microcracks, improving interfacial cohesion and reducing ionic permeability by 2-3 orders of magnitude. This duplex configuration, constituted by a mechanically robust PEO layer and a sol-gel top-coat with superior barrier properties, has been shown to significantly increase impedance values (reaching 10^6-10^7 Ω·cm^2) and markedly reduce corrosion rates in saline or humid environments, with protection efficiencies frequently exceeding 95% [13,28,32].

Despite the extensive literature on PEO/sol-gel duplex systems, several critical knowledge gaps remain unaddressed, hindering the optimization of these promising protective strategies [28–35]. Most studies have relied exclusively on conventional (arc) PEO coatings as the base layer, neglecting the potential influence of the electrical regime on sol-gel infiltration behaviour and interfacial bonding. Although PEO has attracted considerable attention for its ability to generate thick, adherent oxide layers with improved hardness and wear resistance, systematic comparisons between different discharge regimes and their subsequent interaction with sealing or functional sol-gel layers remain limited. In particular, the role of discharge regime in controlling pore architecture and its subsequent influence on sol-gel infiltration, adhesion, and mechanical stability has not been systematically addressed for magnesium alloys [36,37]. This represents a fundamental limitation in understanding how PEO processing parameters influence the performance of the overlying sol-gel. The morphology, roughness and pore size distribution of PEO coatings are known to govern the extent of sol-gel penetration, mechanical interlocking and crack filling. In arc-regime coatings, large open pores can promote deeper infiltration of the sol-gel network, whereas in soft-sparking regimes the smaller and more uniformly distributed pores tend to confine infiltration to a thinner near-surface region but enable more homogeneous coverage [38,39]. However, the consequences of these pore architectures on the durability and tribological behaviour of hybrid PEO/sol-gel systems remain largely unexplored. This interplay between discharge regime and sol-gel infiltration is expected to strongly affect mechanical stability, adhesion strength and long-term corrosion performance of the duplex system on magnesium alloys [13]. A few recent studies on magnesium alloys have quantified the adhesion of PEO/sol-gel systems, reporting pull-off strengths in the order of 10-50 MPa (for well-bonded systems) [40–43], yet these works typically consider a single PEO condition and do not explore the effect of varying the discharge regime. In contrast, both soft sparking behaviour and its interaction with sol-gel sealing have been addressed by a broader body of work for aluminium substrates, including the impact on stiffness, wear resistance and interfacial cohesion [28,35]. A comparable and systematic framework for magnesium alloys is therefore still lacking.

In this context, the present study investigates the influence of PEO electrical regimes (arc and soft-sparking) on the infiltration behaviour and tribological performance of hybrid PEO/sol-gel coating systems developed on AZ31 alloy. Hybrid sol-gel coatings based on tetraethyl orthosilicate (TEOS), 3-(trimethoxysilyl)propyl methacrylate (MAPTMS), methacrylic acid (MAA), and zirconium tetrapropoxide (ZTP) were deposited by dip-coating onto PEO layers produced under both discharge regimes using optimized synthesis conditions that minimize substrate attack during processing. By directly comparing these two PEO architectures as substrates for sol-gel sealing, the study aims to clarify how discharge-controlled pore structures govern sol-gel infiltration, interfacial adhesion, and tribological behaviour in duplex coating systems. The interaction between coating morphology, wettability and tribological response is analysed through a comprehensive combination of morphological, structural and chemical characterisation and dry sliding wear testing, providing useful information for the design of more durable protection systems for magnesium alloys in aerospace and automotive applications.

2. Materials and methods

- Materials

The AZ31 alloy is constituted by (wt.%): 2.5-3.5 Al, 0.7-1.3 Zn, 0.2 Mn, 0.05 Si, 0.05 Cu, 0.04 Ca, 0.005 Fe, 0.1 Ni and balanced Mg, which was supplied by KG Fridman AB (SWEDEN). In order to prepare the substrate for the PEO process (dimensions of the samples: 6 cm × 6 cm x 0.5 cm). First, the substrate was immersed in a concentrated solution of 2 M HNO_3 for 40 s, then in a diluted solution of 0.25 M HNO_3 for 30 s in order to remove surface oxides and contaminants. Finally, they were dried with compressed air.

The following chemicals were used for the synthesis of the sols: 3-(trimethoxysilyl)propyl methacrylate (MAPTMS, 98.0%, Sigma-Aldrich), tetraethyl orthosilicate (TEOS, 99.0%, Sigma-Aldrich), zirconium tetrapropoxide (ZTP, 70%, Sigma-Aldrich), methacrylic acid (MAA, 99.0%, Sigma-Aldrich), 1-propanol (Sigma-Aldrich) and hydrochloric acid (HCl, 37%, AppliChem).

- PEO treatment

A square pulsed bipolar pulsed DC generator (Micronics Systems, France) was used as a power supply to control the amount of charge ratio (RCQ), defined as the ratio of positive to negative charge. The AZ31 alloy (6 cm × 4 cm x 0.5 cm) was used as the working electrode, with a semicircular stainless steel sheet (20 cm × 22 cm x 0.1 cm) serving as the counter electrode. Two RCQ values of 0.98 (soft regime) and 1.33 (arc regime) were used to produce the ceramic coatings, whose the parameters employed are described in the previous work [16], using a duty cycle at a frequency of 66.7 Hz and a process time of 30 min. The PEO bath was constituted by an electrolyte of 8.4 g/L KOH, 10.5 g/L Na_2SiO_3, and 1.7 g/L NaF in deionized water. It was placed in a double-walled vessel of 3 L capacity (Lenz LF150) and kept at a temperature below 20 °C by a cooler machine (VWR MX 7L R-20).

- Sol-gel treatment

The sol-gel composition, previously described by Peter et al. [44], consists of two sol solutions. The first solution (sol 1) was composed of TEOS (0.18 mol) and MAPTMS (1 mol) precursors whose hydrolysis and condensation reactions were initiated by dropwise addition of distilled water (2.075 mol) and hydrochloric acid (0.001 mol), stirring for 2 h. Sol 2 containing ZTP (0.12 mol), MAA (0.12 mol) and 1-propanol alcohol (0.4 mol) was stirred for 30 min. Then, after 2 h and 30 min of total stirring, sol 1 was added drop by drop over sol 2 and stirred for 24 h to ensure the development of the hydrolysis and condensation reactions. After that, the AZ31 alloy and the PEO coated samples were dip-coated in the sol-gel solution for 1 min with a withdrawal speed of 100 mm/min and then cured at 100 °C for 1h. The nomenclature for each sample is represented in the following Table 1.

- *Surface characterization*

The composition and morphology of all the samples were analysed using a scanning electron microscope (SEM, Hitachi SU8020) fitted with a X-ray energy dispersive system (EDX, Thermo Scientific Noran System 7). The cross-section of the samples was prepared by grinding them with SiC abrasive sheets ranging in grit from P240 to P1200 and then polishing them with diamond paste from 3 to 1 μm.

The thickness of the coatings was determined by ten independent measurements taken from cross-sectional micrographs. The average of pore size was determined by evaluating three representative images of the surface, obtained at 1000 × magnification. The image analysis was performed using ImageJ software (National Institutes of Health, USA). Roughness measurements have been achieved by means of the Hirox KH-8700 digital microscope, the mean of five measurements being reported.

The wetting behaviour of the samples was evaluated through sol-gel contact angle measurements using the ZTP precursor solution and a DSA10-MK2 KRÜSS apparatus. Three measurements were performed for each sample to ensure reproducibility. This parameter reflects the sol's affinity for the coating surface, indicating the ease of spreading during deposition.

Table 1
Nomenclature for the samples studied.

Designation	Description of PEO process
Mg/ZTP	-
PEO-AR	Arc PEO regime
PEO-SR	Soft PEO regime
PEO-AR/ZTP	Arc PEO regime + sol-gel
PEO-SR/ZTP	Soft PEO regime + sol-gel

- Fourier transform infrared spectroscopy (FTIR)

In order to obtain a clearer picture of the chemical composition of the sol-gel coatings, the final drops of the solution were dried in an oven at 120 °C and then converted into powder for FTIR analysis using an IRTracer-100 device (Shimadzu Co.), within the wavelength range of 600 to 4000 cm^{-1}.

- Rheological measurement

The flow properties of the sol-gel solution were evaluated at a temperature of 25 ± 0.1 °C using an Anton Paar MCR 302 rheometer with double-space cylinders (in accordance with ISO/WD 3219-2 standards). The evolution of viscosity versus shear rate of 0-200 s^{-1} was previously determined to verify the Newtonian behavior of the ZTP solution. The final solution was then left to age without stirring, and each test was performed twice in order to obtain accurate results.

- Mechanical tests

Tribological tests were performed using a Bruker TriboLab tribometer designed for reciprocal wear, which had an alumina counterweight with a diameter of 4.8 mm. During the tests, a normal load of 2 N was applied at room temperature. The total sliding distance was calculated according to equation L = 2 l·f·t, where the stroke length (l) is 10 mm, frequency (f) is 2 Hz and the time (t) is adjusted to reach 100 m. The coefficients of friction (COF), determined by the ratio between F_t and F_n, were recorded every 0.1 s (where Ft represents the friction force and F_n the normal force).

3. Results and discussion

3.1. Characterization of the ZTP sol-gel precursor by FTIR and rheology

Fig. 1 (a) presents the FTIR spectrum of the ZTP-based hybrid sol-gel coating, organized from high to low wavenumbers to facilitate interpretation of the network structure. In the 3600-3200 cm^{-1} region, a broad absorption band is observed, assigned to –OH stretching vibrations of silanol groups and physiosorbed water, typical intermediates during sol-gel hydrolysis [28,45]. The intensity of this band is indicative of the degree of condensation, with a decrease corresponding to the progressive formation of Si–O–Si and Zr–O–Si bridges within the developing network. The 2950-2890 cm^{-1} bands correspond to asymmetric and symmetric C–H stretching vibrations of the methacrylate groups in MAPTMS and MAA. Their presence confirms the retention of organic functionalities during condensation, which contribute to flexibility and crack mitigation. Simultaneously, the methoxysilane groups participate in hydrolysis-condensation reactions, establishing covalent Si–O–C and Si–C–C linkages that integrate the organic and inorganic domains into a cohesive hybrid matrix. In the 1200-1000 cm^{-1} fingerprint region, characteristic Si–O–Si stretching vibrations dominate [46, 47]. A primary band at 1010 cm^{-1}, accompanied by a shoulder near

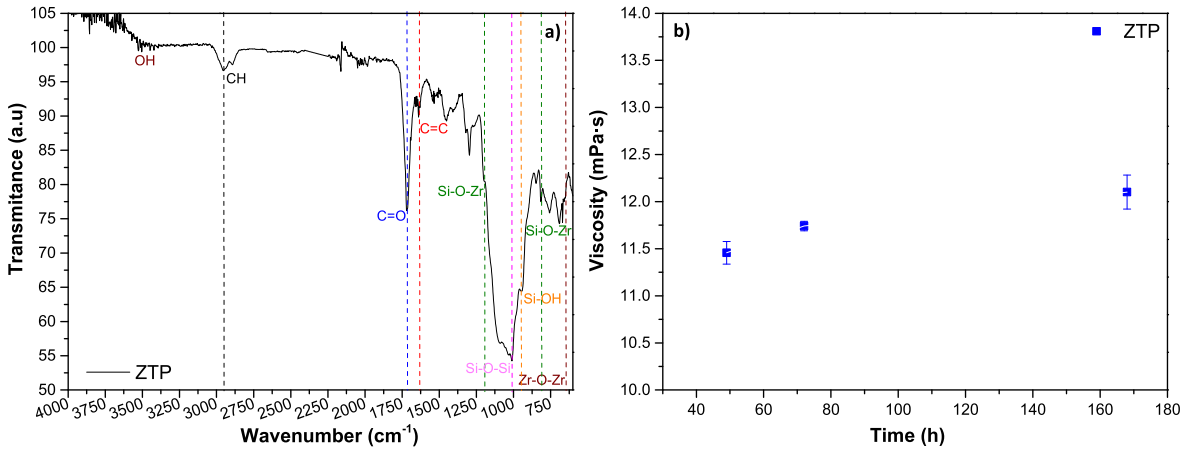

Fig. 1. (a) FTIR spectra and (b) evolution of viscosity as function of ageing time of ZTP solution.

1060-1080 cm^{-1}, indicates the coexistence of ladder-like and cage-like siloxane structures. Ladder-type motifs correspond to linear or cyclic oligomers formed during early condensation stages, whereas cage-like structures result from extensive cross-condensation, generating a denser and more rigid network [48]. The simultaneous presence of both motifs demonstrates the formation of a partially crosslinked inorganic network, consistent with a three-dimensional hybrid architecture. Additionally, bands at 1150-1160 cm^{-1} and near 800 cm^{-1} are attributed to Si–O–Zr hetero-condensation, providing evidence of zirconium integration into the silicate network. This chemical incorporation ensures a uniform co-hybrid structure rather than phase-segregated ZrO_2- or SiO_2-rich domains and contributes to enhanced crosslinking density, thermal and chemical stability, and barrier properties of the final coating. A weaker absorption near 620-660 cm^{-1} is attributed to Zr–O–Zr linkages, thereby confirming partial self-condensation of zirconium species [49].

Overall, the presence of Si–O–Si, Si–O–Zr and Zr–O–Zr bands confirms the formation of a mixed Zr–Si hybrid network rather than separated ZrO_2 or SiO_2 phases, in agreement with previous reports on Zr–Si sol-gel coatings [28,45,50]. The combination of inorganic (Zr–O–Si/Si–O–Si/Zr–O–Zr) and organic (C–H, Si–O–C) signatures indicates an interpenetrated hybrid architecture that is expected to influence both mechanical compliance and adhesion to the underlying PEO layer.

Another critical factor determining the infiltration and sealing efficiency of sol-gel coatings on PEO-treated AZ31 is the viscosity and

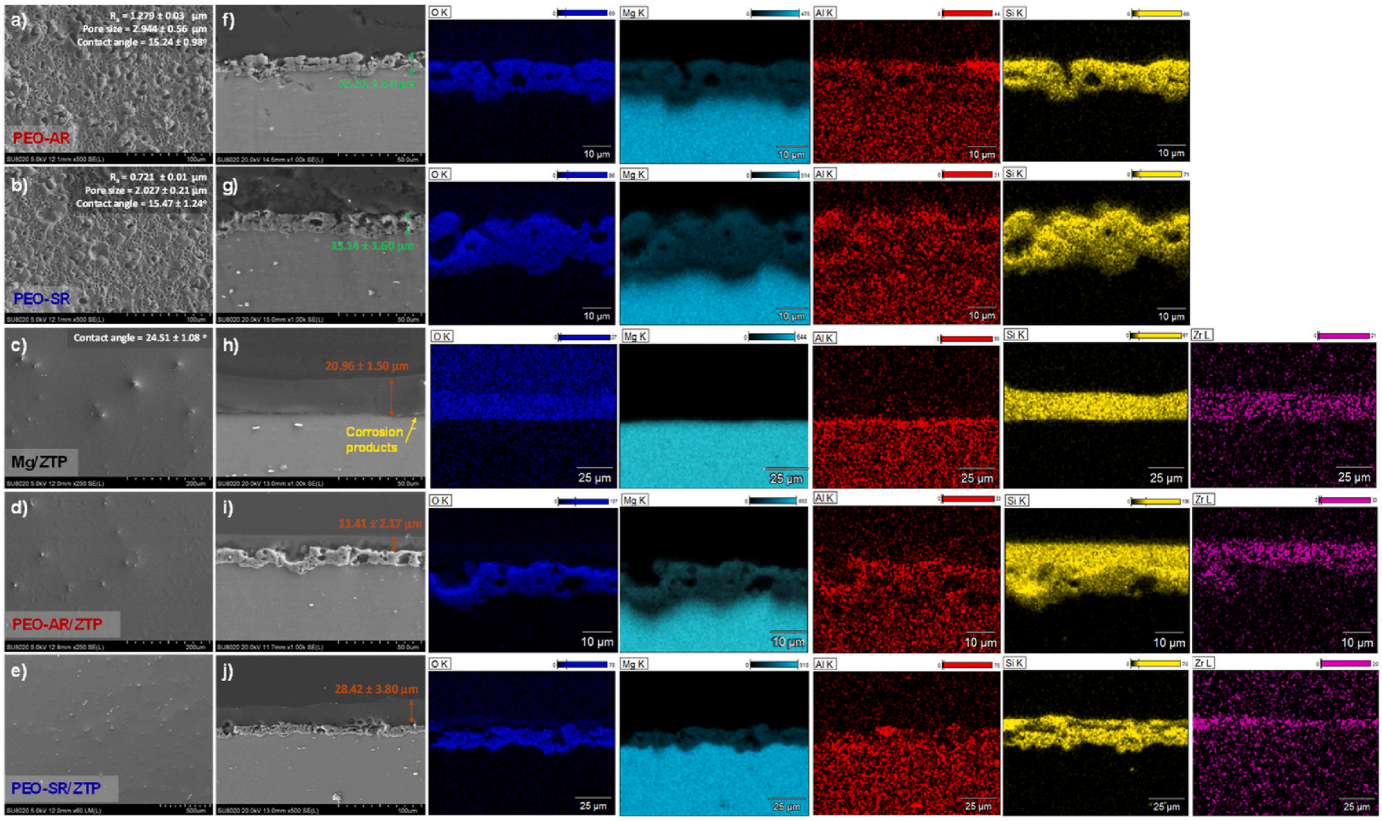

Fig. 2. (a-e) Plan view and (f-j) cross-section of (a, b, f, g) PEO and (c-e, h-j) sol-gel systems in the (a, f, d, i) arc and (b, g, e, j) soft regimes on the AZ31 alloy. EDS mapping illustrations of the samples studied.

evaporation dynamics of the sol-gel precursor [28,45]. Fig. 1 (b) displays the evolution of the ZTP solution as function of ageing time. The viscosity remains nearly constant during the ageing process, with values around ~11.4-12.1 mPa·s at 25 °C, suggesting stable hydrolysis-condensation reactions in the sol that prevent significant changes in the degree of polymerisation. These viscosity values are sufficiently low to allow good wetting and spreading on the PEO-coated surface while still enabling the formation of a continuous sol-gel film [51]. Such values are consistent with partially hydrolysed Zr–Si sol-gel systems reported in the literature [28,45,48]. In duplex PEO/sol-gel coatings, In duplex PEO/sol-gel coatings, this rheological behaviour is important because it governs the balance between surface sealing and pore infiltration within the PEO structure.

3.2. Characterization of the samples

Fig. 2 presents the surface (a-e), cross-sectional (f-j) morphologies and the elemental distribution maps of the bare PEO layers obtained under arc and soft regimes (a, b, f, g), sol-gel deposited directly on magnesium (c, h), and the duplex systems PEO-AR/ZTP (d, i) and PEO-SR/ZTP (e, j). Distinct morphological and structural features are evident between the different treatments, reflecting the influence of the electrical regime and subsequent sol-gel sealing.

- Morphology and structure of the PEO coating

In Fig. 2 (a, b), the PEO coatings produced under the arc (PEO-AR) and soft (PEO-SR) regimes show notable microstructural differences. The PEO-AR surface exhibits large, irregular discharge pores (average diameter ≈ 2.9 ± 0.6 μm) and higher roughness (R_a = 1.28 ± 0.03 μm), indicative of strong plasma activity and localized melting-solidification events. In contrast, the PEO-SR coating displays smaller and more uniformly distributed pores (average diameter ≈ 2.1 ± 0.2 μm) and a significantly smoother surface (R_a = 0.72 ± 0.01 μm), characteristic of controlled micro-discharges typical of the soft regime. These results align with previous studies reporting that soft regimes produce denser, finer-grained oxide layers with up to 40-50 % lower porosity compared to conventional arc regimes [52]. Cross-sectional analysis (Fig. 2 (f and g)) confirms the presence of a typical three-layer structure comprising a dense inner barrier layer, an intermediate transition zone, and an outer porous region. The PEO coating thicknesses were approximately 15.31 ± 3.0 μm (PEO-AR) and 13.14 ± 1.60 μm (PEO-SR), consistent with the lower voltage and discharge energy of the soft regime, which leads to less intense plasma micro-arcs and slower oxide growth [53–55].

- Morphology of sol-gel coated samples

In the case of the sol-gel coated samples, morphological changes become evident (Fig. 2 (c–e)). For the Mg/ZTP sample (Fig. 2 (c)), a flat sol-gel layer is observed on the surface, with some particles trapped beneath the layer, possibly associated with the formation of silica particles. Silica particles could be formed *in situ* during the sol-gel process through the hydrolysis and condensation of silanol derived from TEOS. These reactions generated Si–O–Si bonds, leading to the nucleation and growth of colloidal silica agglomerates. As gelation progressed, the nanoparticles became trapped and integrated into the continuous sol-gel network [56]. According to the cross-sectional of Fig. 2 (h) reveals a homogeneous sol-gel film of 20.96 ± 1.50 μm thickness. However, initial signs of corrosion can be seen in some areas of the substrate, attributed to the acidic nature (pH ≈ 2-3) of the precursor solution accelerating Mg dissolution during deposition, as also reported in previous work [57].

In duplex systems (PEO-AR/ZTP and PEO-SR/ZTP, Fig. 2 (d and e)), the sol-gel layer covers both PEO coatings, producing a smooth, uniformly flat surface in both cases. Additionally, particles embedded in certain regions of the sol-gel matrix have been observed, similar to those in the Mg/ZTP sample. The principal distinctions between the systems are related to the extent of sol-gel infiltration. In PEO-AR/ZTP (Fig. 2 (i)), the sol-gel layer reaches 11.41 ± 2.17 μm, indicating substantial sol-gel penetration into the larger pores and interconnected microcraters that are characteristic of the PEO structure of the arc regime. Conversely, the PEO-SR/ZTP system (Fig. 2 (j)) exhibits a thicker sol-gel coating (28.42 ± 3.80 μm), yet the sol-gel remains predominantly superficial due to the finer and more compact pore network of the soft regime layer, which limits deeper infiltration. These results partially align with literature reports showing duplex PEO/sol-gel coatings on AZ31 in the range of 25-30 μm, although variations in coating thickness are strongly dependent on sol formulation and deposition kinetics. For example, Merino et al. observed hybrid layers of 25-30 μm on AZ31B, while Liu et al. reported 15-20 μm for systems produced using alternative sol-gel formulations [33,34]. The lower thickness measured for the PEO-AR/ZTP sample can be rationalised by considering both the effects of pore morphology and the rheological behaviour of the ZTP solution. The higher porosity and larger discharge pores (>2 μm) characteristic of the arc regime provide open capillary pathways that, which, combined with the moderate viscosity of the ZTP solution (~11.4-12.1 mPa·s), favour deep capillary-driven infiltration rather than simple build-up at the surface. As a result, a significant fraction of the sol penetrates into the porous PEO-AR structure, enhancing mechanical interlocking without greatly increasing the external coating thickness. In contrast, the finer and denser pore network of the PEO-SR layer limits capillary penetration under identical rheological conditions, leading to a more superficial hybrid layer. This behaviour is consistent with previous studies by Pezzato et al. and Toorani and Aliofkhazraei, who demonstrated that incomplete sealing of fine-pore PEO coatings leaves residual channels that can act as preferential corrosion paths [26,58]. Contact angle measurements performed with the ZTP sol showed similar values for the PEO-AR and PEO-SR surfaces (~15 °), indicating comparable wettability of both coatings. Therefore, the capillary infiltration of the sol-gel solution is not primarily governed by differences in surface wettability but rather by the pore size and connectivity of the PEO layers.

EDS elemental mapping revealed that the PEO coatings are mainly composed of Mg, O, and Si, with a lower presence of Al homogeneously distributed across the surface. These elements originate from the AZ31 substrate and the silicate-based electrolyte used during the PEO process. The phase composition of similar coatings produced under soft and arc regimes has been previously reported by our group [16]. X-ray diffraction analysis showed that the coatings mainly consist of Mg, MgO, and Mg_2SiO_4 phases, while no distinct Al-containing phases were detected due to their low concentration. The presence of Mg peaks was attributed to X-ray penetration through the thin and porous coatings, and a slightly higher intensity of Mg_2SiO_4 peaks was observed for the spark regime, likely due to the higher discharge energy and local temperatures promoting increased crystallinity and formation of Mg_2SiO_4. In the case of ZTP-coated systems, the detection of Si, O, Zr and Al across the outer layer confirms the presence of a Zr–Si hybrid film, in agreement with the Zr–O–Si, Si–O–Si and Zr–O–Zr bands identified in the FTIR spectrum (Fig. 1 (a)). SEM-EDS mapping further shows that Zr and Si partially infiltrate the PEO-AR layer, whereas in PEO-SR/ZTP some pores remain free of Zr and Si, consistent with the limited penetration expected from the pore size distribution and sol viscosity. This compositional heterogeneity, already anticipated from the FTIR and rheological characterization, provides a structural basis for the mechanical response that will be discussed in the following section.

3.3. Mechanical properties

The coefficient of friction was measured to evaluate the tribological performance of the PEO coatings, both unsealed (PEO-AR and PEO-SR) and sealed with a sol-gel layer (AZ31/ZTP, PEO-AR/ZTP and PEO-SR/ZTP). Fig. 3 shows the evolution of the friction coefficient (COF) as a

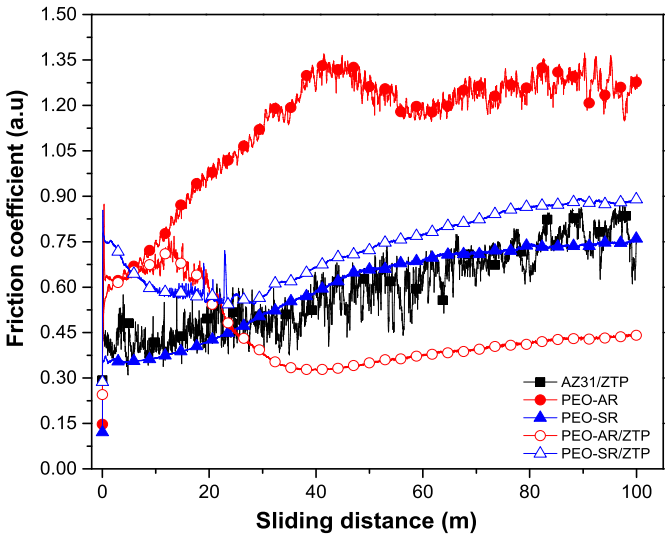

Fig. 3. Friction coefficients after dry sliding wear of treated systems.

function of sliding distance.

For the PEO coatings (PEO-AR, red and filled circles, and PEO-SR, blue and filled triangles), a gradual increase in the friction coefficient is observed, stabilizing at approximately 1.35 for PEO-AR and 0.65 for PEO-SR after 75 m of sliding distance. The lower friction of the PEO-SR coating can be attributed to surface morphology of the PEO coating, which has smoother surface and reduced porosity, while the rougher morphology and presence of more hard MgO and Mg_2SiO_4 phases (as seen in this work [16]) in the PEO-AR layer promote abrasive interactions and higher friction. Despite these differences, neither coating exhibited delamination during testing, as indicated by the absence of sudden oscillations in the friction curves. This signifies stable tribological contact without substrate exposure, which is consistent with previous report [16].

After application of the sol-gel layer on the bare Mg substrate (Mg/ZTP, black and square symbols), an initial increase in friction coefficient is observed due to the presence of the top coating. However, after a short sliding distance of 1.5 m, the friction coefficient drops sharply from 0.5 to 0.35 because the sol-gel layer detaches from the substrate. This is followed by an unstable regime with large oscillations (COF: 0.75) that persists until the end of the test, probably as a result of friction between the alumina ball and the exposed substrate, as seen in our previous work (COF ~ 0.75 for PEO-SR and PEO-AR after reaching the substrate) [16]. In contrast, the duplex PEO coatings sealed with ZTP sol-gel (PEO-AR/ZTP, red and unfilled circles, and PEO-SR/ZTP, blue and unfilled triangles) exhibit significantly improved wear resistance compared to their unsealed counterparts. Two distinct trends are observed in the PEO-SR/ZTP and PEO-AR/ZTP systems: at the beginning of the test the friction coefficient gradually increases, followed by a sharp drop from 0.65 and 0.75 to 0.35 and 0.5 for PEO-AR/ZTP and PEO-SR/ZTP, respectively, similar to the behaviour observed in the Mg/ZTP system. After this drop, the PEO-AR/ZTP system maintains a stable friction value around 0.35 until the end of the test, while for the PEO-SR/ZTP system, a gradual increase of the friction coefficient from 0.5 to 0.8 is observed, closely resembling the behaviour of the PEO-SR sample.

These results suggest that the PEO-AR/ZTP system offers better wear resistance than PEO-SR/ZTP, which contrasts with the trend observed in the unsealed PEO coatings. This difference can be attributed to the combined effects of pore morphology and sol-gel rheology. The higher porosity and larger discharge pores (>2 μm) characteristic of the arc-regime PEO layer, together with the viscosity of the ZTP sol (~11.4-12.1 mPa·s), facilitate deeper penetration of the sol-gel into pores and defects. This promotes stronger mechanical interlocking and improved load distribution during sliding. Similar findings have been reported in the literature on AA2024, where sol-gel layers seal PEO-generated porosity, resulting in improved wear performance and lower friction coefficients due to enhanced mechanical interlocking and surface smoothness [59]. In contrast, the finer and denser pore network of the soft-regime PEO layer, as shown in Fig. 2 (j), restricts sol–gel infiltration. As a result, in the PEO-SR/ZTP system the sol-gel remains mainly on the surface, resulting in weaker mechanical interlocking and lower adhesion. Once the sol-gel layer peels off or wears away, the underlying PEO could be exposed and begin to wear away, causing a progressive increase in the coefficient of friction. These results coincide with the conclusions of Sopchenski et al., who observed a 40% reduction in the wear rate of sol-gel sealed PEO coatings on AA2024 when effective pore filling occurred [27]. Similarly, Akbarzadeh et al. demonstrated that the effectiveness of sol-gel sealing depends mainly on the depth of penetration, and that sealing only on the surface offers limited tribological advantages [28]. The mechanical interlocking mechanism proposed for PEO-AR/ZTP is supported by the work of Curran and Clyne, who demonstrated that porosity and microcracks in PEO coatings reduce stiffness by an order of magnitude, but that effective filling with compatible materials can still achieve mechanical integrity [60].

Fig. 4 presents the SEM images of the samples after the wear test. In the PEO-AR sample (Fig. 4 (a)), the wear track is characterized by a broad appearance and a smoother morphology relative to the surrounding surface, indicative of abrasive wear. This finding is consistent with the higher coefficient of friction (COF = 1.35) previously observed and is corroborated by EDS analysis showing elevated Mg, O, and Si concentrations (Table 2, point 1-3), thus could confirming the presence of ceramic phases such as MgO and Mg_2SiO_4. These phases may act as lubricants, but simultaneously promote abrasive interactions, thereby increasing both friction and material loss. In contrast, the PEO-SR sample (Fig. 4 (c)), displays a more constricted and less well-defined wear track, indicating a reduced wear volume. This finding is consistent with the lower COF (0.65) and it is supported by EDS analysis revealing a more homogeneous composition with lower Si content (Table 2, points 4-6), which suggests reduced abrasion and more stable sliding conditions. In addition, small amounts of Mg and Si are detected in the alumina ball (point 3 and 6, Table 2) of both PEO-coated samples, which is characteristic of adhesion wear. The absence of significant delamination or microcracks further suggests that there is robust mechanical integrity under tribological loading. The results of this study corroborate the hypothesis that the PEO-SR coating exhibits superior wear resistance compared to the PEO-AR coating. This phenomenon can be attributed to the smoother, less porous morphology and thinner structure of the PEO-SR coating, which minimize mechanical interlocking between the sample and the alumina ball, thereby reducing friction forces.

In the case of the sealed samples, the presence of the sol-gel layer (ZTP) significantly influences wear morphology and tribological performance in comparison to unsealed coatings. In the Mg/ZTP sample (Fig. 4 (e, f) and points 7-11 in Table 2), the wear track exhibits deep grooves, sharp boundaries, and pronounced debris accumulation, indicating substantial material loss. The debris (Table 2, point 8) are composed of oxygen, meaning that the substrate underwent oxidation due to the temperature increase occurring during the dry sliding wear test. Moreover, magnesium is observed in the alumina ball due to the adhesion of the substrate on the Al_2O_3 counterbody, corroborating the removal of the sol-gel layer. The observed wear mechanisms are attributable to direct substrate/alumina ball contact following the rapid degradation of the sol-gel layer, which provides minimal protection. This is consistent with the observed reduction in friction during the testing process, which was subsequently followed by a period of instability resulting from progressive exposure to the Mg substrate. In contrast, the PEO-AR/ZTP system (Fig. 4 (g, h) and points 12-14 in Table 2) demonstrates a more stable and narrower wear track than that of the Mg/ZTP sample, with reduced material accumulation (Fig. 4 (g),

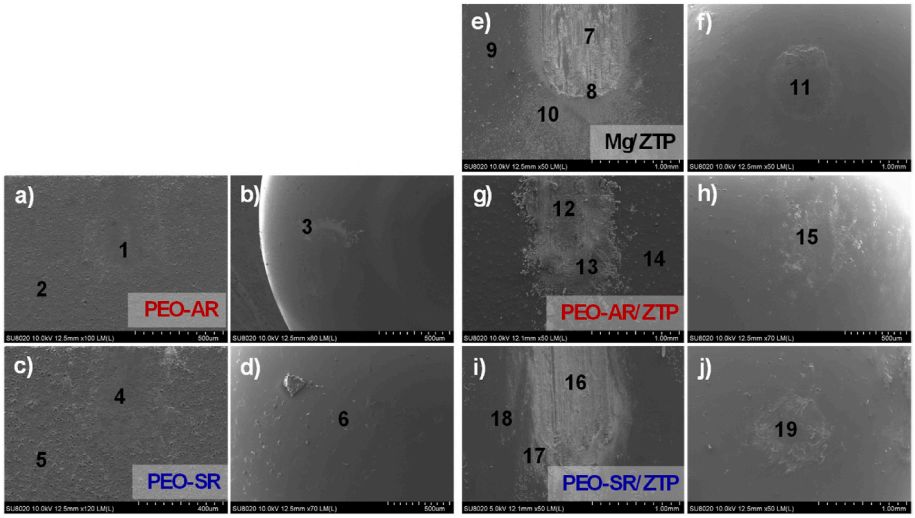

Fig. 4. SEM of (a, c) PEO system and (e, g, i) sol-gel systems after wear test. (b,d,f,h,j) SEM pictures of the alumina counter-body ball.

Table 2
EDS (at.%) analysis of the samples after wear test.

Sample	Location	C	O	F	Na	Mg	Al	Si	Zr
PEO-AR	1	1.6	55.0	0.7	0.5	30.8	1.6	9.9	-
	2	1.6	51.4	0.3	1.1	33.5	1.3	11.0	-
	3	3.8	39.6	-	-	51.3	4.9	-	-
PEO-SR	4	1.4	55.1	0.5	0.8	30.8	1.6	9.0	-
	5	2.3	51.8	0.8	0.8	31.4	1.3	10.9	-
	6	6.5	56.5	-	-	-	36.7	-	-
AZ31/ZTP	7	1.3	20.1	-	-	76.3	2.3	-	-
	8	1.5	43.0	-	-	53.7	1.8	-	-
	9	28.6	46.3	-	-	8.0	-	15.8	1.3
	10	34.6	46.6	-	-	0.4	-	17.0	1.5
	11	7.6	61.6	-	-	30.1	0.4	0.9	0.7
PEO-AR/ZTP	12	3.2	54.6	0.5	-	29.6	1.8	10.3	-
	13	12.3	57.0	-	-	15.8	2.3	11.9	0.7
	14	36.4	44.8	-	-	0.7	-	16.7	1.4
	15	4.2	58.8	-	-	1.9	33.9	0.8	0.3
PEO-SR/ZTP	16	12.0	45.3	-	-	32.1	1.2	9.5	-
	17	1.8	19.4	-	-	65.7	1.9	10.4	-
	18	36.4	45.6	-	-	0.3	-	16.3	1.4
	19	27.3	41.7	-	-	15.1	1.5	13.2	1.2

point 13 in Table 2) corresponding to the accumulation of the sol-gel coating. This behaviour can be attributed to the higher porosity and larger discharge pores of the arc-regime PEO coating, which promote deeper infiltration of the sol-gel into the oxide structure. The penetration of the ZTP sol into these interconnected pores enhances mechanical interlocking and improves the interfacial adhesion between the sealing layer and the PEO substrate. As a result, the load applied during sliding can be more effectively distributed within the hybrid PEO/sol-gel structure, leading to enhanced wear resistance and a lower, more stable coefficient of friction (~0.35), compared with the higher friction observed for the unsealed PEO-AR coating (~1.35). In addition, partial pore filling and surface smoothing reduce the abrasive character of the PEO topography by sealing micro-defects and reinforcing the structural integrity of the coating.

However, in the case of the PEO-SR/ZTP sample (Fig. 4 (i, j), points 16-19 in Table 2), a greater and more degraded wear track was observed than in the unsealed PEO-SR coating, with clear signs of surface alteration and the presence of wear material (Fig. 4 (j), point 16 vs. 17 in Table 2) corresponding to the accumulation of high Mg, Zr, and Si content at the scratch edges, which corresponds to the accumulation of the PEO and sol-gel coating. The progressive increase in the friction coefficient from approximately 0.6 to 0.8, as observed in this soft regime system, indicates that the sol-gel layer, although initially present, offers limited long-term protection. This behaviour can be related to the finer and more compact pore network characteristic of the soft-sparking PEO coating. The reduced pore size restricts sol-gel infiltration and limits the formation of strong mechanical interlocking within the oxide layer. Consequently, the sol-gel remains predominantly as a superficial film, which is more susceptible to delamination during sliding. This interpretation is supported by the higher Si and Zr content detected on the alumina ball (point 17 in Table 2) for the PEO-SR/ZTP system compared with PEO-AR/ZTP (Si: 13.2 vs 0.8 at.% and Zr: 1.2 vs 0.3 at.%), indicating greater removal of the sol-gel layer during wear.

Overall, the results indicate that the arc regime (PEO-AR) promotes more effective sol-gel infiltration into the porous oxide structure due to its coarser pore network (>2 μm channels). This enhanced infiltration improves the mechanical interlocking between the PEO layer and the sol-gel coating, contributing to smoother wear tracks and more stable friction behaviour despite moderately higher wear rates. These findings highlight the importance of the initial PEO pore architecture in controlling the performance of hybrid PEO/sol-gel duplex coatings.

4. Conclusions

The results demonstrate that the microstructural and morphological characteristics of the PEO layers, determined by the electrical deposition

regime, play a decisive role in the infiltration of the sol-gel coating and therefore in the mechanical performance of the PEO/sol-gel duplex coatings. PEO coatings formed under the arc regime exhibited larger pores and higher surface roughness, whereas those obtained under the soft regime developed denser and smoother oxide structures. FTIR confirmed the formation of a hybrid Zr–Si network composed of Zr–O–Si, Si–O–Si, and Zr–O–Zr linkages, while rheological measurements revealed a nearly constant response with moderate viscosity, favouring infiltration into porous ceramic architectures. These chemical and rheological characteristics were essential in governing the extent of pore filling and interfacial bonding. In the duplex configurations, the sol-gel effectively sealed the porous PEO architecture, with deeper infiltration in the PEO-AR coatings leading to improved wear resistance, better load distribution, and higher interfacial cohesion. The PEO-AR/ZTP system demonstrated the most stable and lowest friction coefficient (~0.35) and exhibited minimal wear track damage, thus confirming the mechanical advantages of efficient sol-gel interlocking and network reinforcement. In contrast, the PEO-SR/ZTP coatings exhibited minimal sol-gel penetration and progressive degradation under sliding, suggesting reduced long-term stability. These findings emphasise the significance of optimising the relationship between PEO microstructure, sol-gel viscosity, and infiltration kinetics to customise the tribological response of duplex coatings. The results obtained provide a comprehensive understanding of how coating architecture and interfacial bonding govern performance, thus offering a foundation for the rational design of advanced hybrid protective systems.

CRediT authorship contribution statement

Lara Moreno: Writing-original draft, Methodology, Investigation, Formal analysis, Conceptualization, Funding acquisition. Alexandre Mégret: Validation, Investigation, Formal analysis. Yoann Paint: Validation, Investigation. Marie-Georges Olivier: Writing-review & editing, Validation, Supervision, Methodology, Funding acquisition, Conceptualization.

Funding and acknowledgements

This research has been funded by the Belgian government through the University of Mons (UMONS), as part of the Come to Wallonia (C2W, Horizon 2020 European Union Funding for Research and Innovation) grant programme, which was attributed to Lara Moreno. The C2W grant has been the beneficiary of funding from the European Union's Horizon 2020 research and innovation programme, under the Marie Skłodowska Curie grant agreement No. 101034383.

Declaration of competing interest

The authors declare that they have no known competing financial interests or personal relationships that could have appeared to influence the work reported in this paper.

References

[1] Zhang J, Miao J, Balasubramani N, Cho DH, Avey T, Chang C-Y, et al. Magnesium research and applications: past, present and future. J Magnesium Alloys 2023;11:3867–95. https://doi.org/10.1016/j.jma.2023.11.007.
[2] Zhan L, Kong C, Zhao C, Cui X, Zhang L, Song Y, et al. Recent advances on magnesium alloys for automotive cabin components: materials, applications, and challenges. J Mater Res Technol 2025;36:9924–61. https://doi.org/10.1016/j.jmrt.2025.05.105.
[3] Bai J, Yang Y, Wen C, Chen J, Zhou G, Jiang B, et al. Applications of magnesium alloys for aerospace: a review. J Magnesium Alloys 2023;11:3609–19. https://doi.org/10.1016/j.jma.2023.09.015.
[4] Kwon G-R, Woo SH, Lim S-R. Industrial ecology-based strategies to reduce the embodied CO2 of magnesium metal. Resour Conserv Recycl 2015;104:206–12. https://doi.org/10.1016/j.resconrec.2015.08.008.
[5] Dieringa H, StJohn D, Pérez Prado MT, Kainer KU. Editorial: latest developments in the field of magnesium alloys and their applications. Front Mater 2021;8. https://doi.org/10.3389/fmats.2021.726297.
[6] Kulekci MK. Magnesium and its alloys applications in automotive industry. Int J Adv Manuf Technol 2008;39:851–65. https://doi.org/10.1007/s00170-007-1279-2.
[7] Atrens A, Shi Z, Mehreen SU, Johnston S, Song G-L, Chen X, et al. Review of Mg alloy corrosion rates. J Magnesium Alloys 2020;8:989–98. https://doi.org/10.1016/j.jma.2020.08.002.
[8] Zhang T, Wu S, Liu H, Yang L, Chen T, Wang X, et al. Research on comparative marine atmospheric corrosion behavior of AZ31 magnesium alloy in South China Sea. Materials 2025;18:3585. https://doi.org/10.3390/ma18153585.
[9] Zeng R, Zhang J, Huang W, Dietzel W, Kainer KU, Blawert C, et al. Review of studies on corrosion of magnesium alloys. Trans Nonferrous Met Soc China 2006;16:s763–71. https://doi.org/10.1016/S1003-6326(06)60297-5.
[10] Saji VS. Electrolyte and electrolyte-additives for improved plasma electrolytic oxidation on magnesium alloys. Appl Surf Sci Adv 2025;26:100700. https://doi.org/10.1016/j.apsadv.2025.100700.
[11] Acquesta A, Russo P, Schino A, Stornelli G, Monetta T. Plasma electrolytic oxidation treatment on magnesium rare Earth alloy: effect of low current density. Adv Eng Mater 2024;26. https://doi.org/10.1002/adem.202401480.
[12] Lashkarara S, Fazlali A, Ghaseminezhad K, Fleck C, Salavati M. Mechanism of plasma electrolytic oxidation in Mg3ZnCa implants: a study of double-layer formation and properties through nanoindentation. Sci Rep 2024;14:7380. https://doi.org/10.1038/s41598-024-58008-8.
[13] Fattah-alhosseini A, Fardosi A, Askari A, Karbasi M, Dikici B, Kaseem M. Enhancing Plasma Electrolytic Oxidation (PEO) coatings on magnesium alloys: the critical role of surface pretreatments. Adv Mater Interfac 2025;12:2500192. https://doi.org/10.1002/admi.202500192.
[14] Zhou P, Li C, Jiao G, Lv T, Zhang T, Wang F. Bridge for the thermodynamics and kinetics of electrochemical corrosion: the design of self-densified plasma electrolytic oxidation coating on Mg alloys. J Mater Sci Technol 2025;216:66–80. https://doi.org/10.1016/j.jmst.2024.07.040.
[15] Martin J, Nominé AV, Stef J, Nominé A, Zou JX, Henrion G, et al. The influence of metallurgical state of substrate on the efficiency of plasma electrolytic oxidation (PEO) process on magnesium alloy. Mater Des 2019;178:107859. https://doi.org/10.1016/j.matdes.2019.107859.
[16] Moreno L, Mégret A, Paint Y, Gonon M, Vitry V, Olivier M-G. Comparison of spark and soft regimes in the PEO process in terms of corrosion and wear performance of AZ31 alloy for biomedical applications. Mater Today Commun 2025;42:111440. https://doi.org/10.1016/j.mtcomm.2024.111440.
[17] Pietrzyk S, Gębarowski W. Stability of the soft sparking state in the plasma electrolytic oxidation process. Materials 2025;18:989. https://doi.org/10.3390/ma18050989.
[18] Sikdar S, Menezes PV, Maccione R, Jacob T, Menezes PL. Plasma electrolytic oxidation (PEO) process—processing, properties, and applications. Nanomaterials 2021;11:1375. https://doi.org/10.3390/nano11061375.
[19] Kamil MP, Kaseem M, Ko YG. Soft plasma electrolysis with complex ions for optimizing electrochemical performance. Sci Rep 2017;7. https://doi.org/10.1038/srep44458.
[20] Hu P, Wei B, Cheng Y, Cheng Y. Discharge channel structure revealed by plasma electrolytic oxidation of AZ31Mg alloy with magnetron sputtering Al layer and corrosion behaviors of treated alloy. Trans Nonferrous Met Soc China 2024;34:139–56. https://doi.org/10.1016/S1003-6326(23)66387-3.
[21] Zhao C, Wang X, Yu B, Cai M, Yu Q, Zhou F. Research progress on the wear and corrosion resistant plasma electrolytic oxidation composite coatings on magnesium and its alloys. Coatings 2023;13. https://doi.org/10.3390/coatings13071189.
[22] Mashtalyar DV, Nadaraia KV, Imshinetskiy IM, Sinebryukhov SL, Gnedenkov SV. New approach to formation of coatings on Mg–Mn–Ce alloy using a combination of plasma treatment and spraying of fluoropolymers. J Magnesium Alloys 2022;10:1033–50. https://doi.org/10.1016/j.jma.2021.07.020.
[23] Castellanos A, Altube A, Vega JM, García-Lecina E, Díez JA, Grande HJ. Effect of different post-treatments on the corrosion resistance and tribological properties of AZ91D magnesium alloy coated PEO. Surf Coat Technol 2015;278:99–107. https://doi.org/10.1016/j.surfcoat.2015.07.017.
[24] Usmaniya N, Radhakrishna Pillai S, Palanivel M, Edalacheruvu L, Chennampalli P, Vaithiyanathan P, et al. Effect of polycaprolactone coating on the corrosion and biological characteristics of plasma electrolytic oxidised ZM21 magnesium alloy. Surf Coat Technol 2023;471:129915. https://doi.org/10.1016/j.surfcoat.2023.129915.
[25] N U, T Bm, Vs V, M N, Rk L, R N. Assessment of biocorrosion and cytocompatibility of sol-gel deposited ceramic particles on plasma electrolytic oxidised ZM21 alloy for temporary orthopaedic implant application. Surf Coat Technol 2026;523:133232. https://doi.org/10.1016/j.surfcoat.2026.133232.
[26] Toorani M, Aliofkhazraei M. Review of electrochemical properties of hybrid coating systems on Mg with plasma electrolytic oxidation process as pretreatment. Surf Interfaces 2019;14:262–95. https://doi.org/10.1016/j.surfin.2019.01.004.
[27] Sopchenski L, Robert J, Touzin M, Tricoteaux A, Olivier M-G. Improvement of wear and corrosion protection of PEO on AA2024 via sol-gel sealing. Surf Coat Technol 2021;417:127195. https://doi.org/10.1016/j.surfcoat.2021.127195.
[28] Akbarzadeh S, Paint Y, Olivier M-G. A comparative study of different sol-gel coatings for sealing the plasma electrolytic oxidation (PEO) layer on AA2024 alloy. Electrochim Acta 2023;443:141930. https://doi.org/10.1016/j.electacta.2023.141930.

[29] Ren L, Tsuru K, Hayakawa S, Osaka A. Novel approach to fabricate porous gelatin–siloxane hybrids for bone tissue engineering. Biomaterials 2002;23:4765–73. https://doi.org/10.1016/S0142-9612(02)00226-0.
[30] Ahmadipour M, Mohammadi Hossein, Pang Ai Ling, Arjmand Mohammad, Otitoju Ayode, Tunmise U, Okoye Patrick, et al. A review: silicate ceramic-polymer composite scaffold for bone tissue engineering. Int J Polym Mater Polym Biomater 2022;71:180–95. https://doi.org/10.1080/00914037.2020.1817018.
[31] Li Q. 17 - sol-gel coatings to improve the corrosion resistance of magnesium (Mg) alloys. In: Song G-L, editor. Corros. Prev. Magnes. Alloys. Woodhead Publishing; 2013. p. 469–85. https://doi.org/10.1533/9780857098962.3.469.
[32] Chen Z, Geng X, Yong X, Chen X, Sun Z. Microstructural changes of the peo coating induced by silane-based sol–gel treatment. Surf Rev Lett 2022;29:2250098. https://doi.org/10.1142/S0218625X22500986.
[33] Merino E, El Tawil M, Sobrados I, Durán A, Castro Y. In-vitro degradation behavior of hybrid epoxy-alkyl sol–gel/anodized composite coating on AZ31B Mg alloy. J Sol Gel Sci Technol 2025;114:139–47. https://doi.org/10.1007/s10971-022-06012-7.
[34] Liu Y, Cheng X, Wang X, Sun Q, Wang C, Di P, et al. Micro-arc oxidation-assisted sol-gel preparation of calcium metaphosphate coatings on magnesium alloys for bone repair. Mater Sci Eng C 2021;131:112491. https://doi.org/10.1016/j.msec.2021.112491.
[35] Pezzato L, Rigon M, Martucci A, Brunelli K, Dabalà M. Plasma electrolytic oxidation (PEO) as pre-treatment for sol-gel coating on aluminum and magnesium alloys. Surf Coat Technol 2019;366:114–23. https://doi.org/10.1016/j.surfcoat.2019.03.023.
[36] Gobara M, Naeem I, Sheashea M, Correa-Duarte MA, Elbasuney S. Eu-substituted hydroxyapatite/silica sol-gel treatment for corrosion protection of AZ31 magnesium alloy. Ceram Int 2024;50:32051–63. https://doi.org/10.1016/j.ceramint.2024.06.010.
[37] Ivanou DK, Yasakau KA, Kallip S, Lisenkov AD, Starykevich M, Lamaka SV, et al. Active corrosion protection coating for a ZE41 magnesium alloy created by combining PEO and sol–gel techniques. RSC Adv 2016;6:12553–60. https://doi.org/10.1039/C5RA22639B.
[38] Fernández-Hernán JP, López AJ, Torres B, Martínez-Campos E, Matykina E, Rams J. Anticorrosion and cytocompatibility assessment of graphene-doped hybrid silica and plasma electrolytic oxidation coatings for biomedical applications. ACS Biomater Sci Eng 2021;7:5861–77. https://doi.org/10.1021/acsbiomaterials.1c00326.
[39] Ibrahim H, Dehghanghadikolaei A, Advincula R, Dean D, Luo A, Elahinia M. Ceramic coating for delayed degradation of Mg-1.2Zn-0.5Ca-0.5Mn bone fixation and instrumentation. Thin Solid Films 2019;687:137456. https://doi.org/10.1016/j.tsf.2019.137456.
[40] Merino E, Durán A, Castro Y. Integrated corrosion-resistant system for AZ31B Mg alloy via plasma electrolytic oxidation (PEO) and sol-gel processes. Int J Appl Glass Sci 2021;12:519–30. https://doi.org/10.1111/ijag.16536.
[41] Toorani M, Aliofkhazraei M, Mahdavian M, Naderi R. Superior corrosion protection and adhesion strength of epoxy coating applied on AZ31 magnesium alloy pre-treated by PEO/silane with inorganic and organic corrosion inhibitors. Corros Sci 2021;178:109065. https://doi.org/10.1016/j.corsci.2020.109065.
[42] Parichehr R, Dehghanian C, Nikbakht A. Preparation of PEO/silane composite coating on AZ31 magnesium alloy and investigation of its properties. J Alloys Compd 2021;876:159995. https://doi.org/10.1016/j.jallcom.2021.159995.
[43] H S, G S. S. A, M. A, N. R. Fabrication of duplex coatings on biodegradable AZ31 magnesium alloy by integrating cerium conversion (CC) and plasma electrolytic oxidation (PEO) processes. J Alloys Compd 2017;722:698–715. https://doi.org/10.1016/j.jallcom.2017.06.119.
[44] Rodič P, Iskra J, Milošev I. A hybrid organic-inorganic sol-gel coating for protecting aluminium alloy 7075-T6 against corrosion in Harrison's solution. J Sol Gel Sci Technol 2014;70:90–103. https://doi.org/10.1007/s10971-014-3278-8.
[45] Nguyen TT, Thai TT, Paint Y, Trinh AT, Olivier M-G. Effect of cerium nitrate concentration on corrosion protection of hybrid organic/inorganic Si/Zr sol-gel coating applied on hot-dip galvanized steel. Surf Coat Technol 2024;480:130562. https://doi.org/10.1016/j.surfcoat.2024.130562.
[46] Shimojima A, Kuroda K. Alkoxy- and silanol-functionalized cage-type oligosiloxanes as molecular building blocks to construct nanoporous materials. Molecules 2020;25. https://doi.org/10.3390/molecules25030524.
[47] Tagliazucca V, Callone E, Dirè S. Influence of synthesis conditions on the cross-link architecture of silsesquioxanes prepared by in situ water production route. J Sol Gel Sci Technol 2011;60:236–45. https://doi.org/10.1007/s10971-011-2599-0.
[48] Rodič P, Milošev I, Lekka M, Andreatta F, Fedrizzi L. Corrosion behaviour and chemical stability of transparent hybrid sol-gel coatings deposited on aluminium in acidic and alkaline solutions. Prog Org Coating 2018;124:286–95. https://doi.org/10.1016/j.porgcoat.2018.02.025.
[49] Mitkova E, Stambolova I, Stoyanova D, Toteva V, Dimitrov O. Correlation between aging time period of metal precursor sol – phase composition and textural properties of zirconia nanopowders. J Chem Technol Metall 2024;59:223–30. https://doi.org/10.59957/jctm.v59.i1.2024.26.
[50] Castro Y, Aparicio M, Moreno R, Duran A. Silica-zirconia sol-gel coating obtained by different synthesis routes. J Sol Gel Sci Technol 2005;35:41–50. https://doi.org/10.1007/s10971-005-3213-0.
[51] Debecker DP, Mutin PH. Non-hydrolytic sol–gel routes to heterogeneous catalysts. Chem Soc Rev 2012;41:3624–50. https://doi.org/10.1039/C2CS15330K.
[52] Gebarowski W, Pietrzyk S. Influence of the cathodic pulse on the formation and morphology of oxide coatings on aluminium produced by plasma electrolytic oxidation/Wpływ Impulsu Katodowego Na Tworzenie I Morfologie Warstw Tlenkowych Na Aluminium Otrzymywanych Na Drodze Plazmowego Utleniania Elektrolitycznego. Arch Metall Mater 2013;58. https://doi.org/10.2478/v10172-012-0180-7.
[53] Tjiang F, Ye L-W, Huang Y-J, Chou C-C, Tsai D-S. Effect of processing parameters on soft regime behavior of plasma electrolytic oxidation of magnesium. Ceram Int 2017;43:S567–72. https://doi.org/10.1016/j.ceramint.2017.05.179.
[54] Cheng Y, Feng T, Cheng Y. A systematic study of the role of cathodic polarization and new findings on the soft sparking phenomenon from plasma electrolytic oxidation of an al-cu-li alloy. J Electrochem Soc 2022;169:071505. https://doi.org/10.1149/1945-7111/ac82cc.
[55] Martin J, Nominé A, Brochard F, Briançon J-L, Noël C, Belmonte T, et al. Delay in micro-discharges appearance during PEO of Al: evidence of a mechanism of charge accumulation at the electrolyte/oxide interface. Appl Surf Sci 2017;410:29–41. https://doi.org/10.1016/j.apsusc.2017.03.088.
[56] Dixit CK, Bhakta S, Kumar A, Suib SL, Rusling JF. Fast nucleation for silica nanoparticle synthesis in sol-gel method. Nanoscale 2016;8:19662–7. https://doi.org/10.1039/c6nr07568a.
[57] Ng W, Chiu K, Cheng F. Effect of pH on the in vitro corrosion rate of magnesium degradable implant material. Mater Sci Eng C 2010;30:898–903. https://doi.org/10.1016/j.msec.2010.04.003.
[58] Pezzato L, Brunelli K, Gross S, Magrini M, Dabalà M. Effect of process parameters of plasma electrolytic oxidation on microstructure and corrosion properties of magnesium alloys. J Appl Electrochem 2014;44:867–79. https://doi.org/10.1007/s10800-014-0695-x.
[59] Akbarzadeh S, Klumpp RE, Mégret A, Ölmez V, Vitry V, Olivier M-G. Breakthrough in aluminum protection: electrochemical and wear insights into sol-gel sealed PEO-coated AA2024-T3 and AA2198-T851. Surf Coat Technol 2024;494:131510. https://doi.org/10.1016/j.surfcoat.2024.131510.
[60] Curran JA, Clyne TW. Thermo-physical properties of plasma electrolytic oxide coatings on aluminium. Surf Coat Technol 2005;199:168–76. https://doi.org/10.1016/j.surfcoat.2004.09.037.